Journal of Oceanography, Vol. 61, pp. 761 to 773, 2005

Seasonal/Spatial Variations of the Near-Inertial Oscillations in the Deep Water of the Japan Sea

Kosuke Mori[1]*, Takeshi Matsuno[2] and Tomoharu Senjyu[2]

[1]*Department of Earth System Science and Technology, Interdisciplinary Graduate School of Engineering Sciences, Kyushu University, Kasuga, Fukuoka 816-8580, Japan*
[2]*Research Institute for Applied Mechanics, Kyushu University, Kasuga, Fukuoka 816-8580, Japan*

(Received 15 June 2004; in revised form 3 December 2004; accepted 4 December 2004)

A general description of the near-inertial oscillations in the deep water of the Japan Sea has been found by analyzing observed current data accumulated over a period of ten years. The near-inertial oscillations were dominant in the deep water, and those in the southern Japan Sea, the Tsushima current region, were more energetic than those in the northern area. Their temporal variations have an annual cycle with wintertime intensifications corresponding to the windy season over the Japan Sea. In the Yamato Basin, however, the power of the near-inertial oscillations was small during spring and large during summer, in addition to the above seasonal variations. The results of a slab model showed that the wind stress could account for part of the long periodic variations such as the annual cycle of the near-inertial oscillations in the deep water, but this is not expected to be their only source. Since the surface currents in the southern Japan Sea, especially in the Yamato Basin, vary significantly both temporally and spatially, the surface layer itself also could be responsible for the generation of the near-inertial oscillations in the deep water.

Keywords:
· Japan Sea,
· near-inertial oscillation,
· deep water,
· slab model.

1. Introduction

The Japan Sea is one of the marginal seas located in the western part of the North Pacific Ocean. The maximum depth of the Japan Sea is about 3700 m while that of the straits connecting it to the East China, the Pacific and the Okhotsk Seas, is less than 150 m (see Fig. 1). The water below the main pycnocline, lying at a depth of a few hundred meters, is therefore separated from the surrounding seas and is filled with highly homogeneous water of low potential temperature (<1.0°C) and low salinity (~34.06 psu), called the Japan Sea Proper Water (JSPW) (Uda, 1934).

The surface water entering the Tsushima Strait spreads over the southern Japan Sea bounded by the subpolar front at about 40°N, and then converges around the western side of the Tsugaru Strait. It flows out through the Tsugaru and Soya Straits, and the rest flows northward. The main path of the surface flow south of the subpolar front, called the Tsushima Warm Current (TWC), is not distinguishable in a snapshot, and the hydrological characteristics are highly heterogeneous. The TWC is composed of a few transient branches after entering the Japan Sea (Suda *et al*., 1932; Uda, 1934; Tanioka, 1962; Moriyasu, 1972; Naganuma, 1977). In this area, the southern part of the Japan Sea, several warm eddies/meanders are repeatedly being generated and are decaying (Isoda, 1994). Such activity would affect the flow pattern of the TWC.

The current speed in deep water had been estimated to be low, due to the horizontally uniform density distribution of the JSPW (e.g., Ohwada and Tanioka, 1972). Direct current measurements in the deep water, however, have revealed that the deep flow is rather energetic (Takematsu *et al*., 1999a, b; Mori *et al*., 2001; Senjyu *et al*., 2005): the maximum speed occasionally exceeds 15 cm/s. Takematsu *et al*. (1999a, b) showed that the deep currents in the northern Japan Sea are eventful with vertical coherency, and have suggested that such events would arise from the passage of the barotropic eddies. Mori *et al*. (2001) reported that the barotropic currents west of the Tsugaru Strait have periodicities of 26–30, 15–18 and 10–12 days, but they made no mention of other variations with much shorter periods. Senjyu *et al*. (2005) suggested that there is generally an anticlockwise circulation in each basin, that is, the Japan, Yamato, and Ulleung Basins.

* Corresponding author. E-mail: mori@riam.kyushu-u.ac.jp

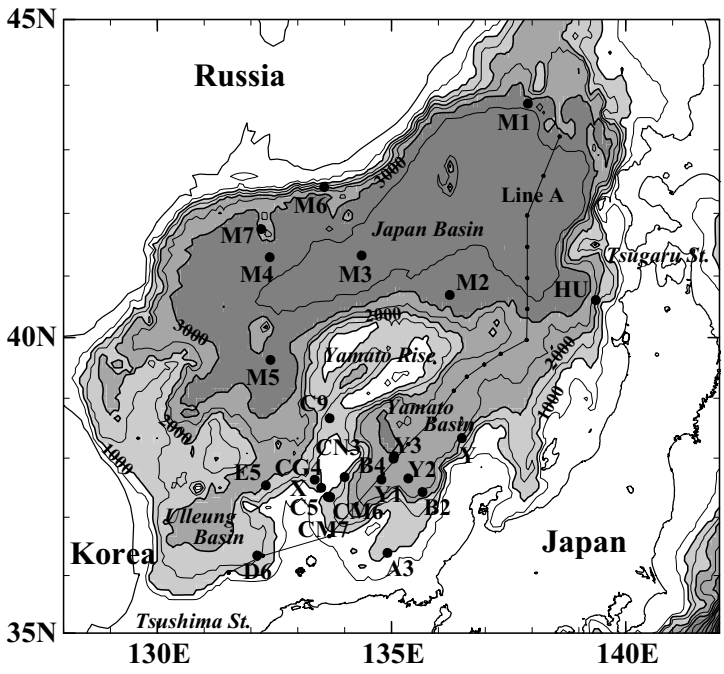

Fig. 1. Bottom topography and the mooring sites. Thin line (Line A) denotes the stations corresponding to the hydrographic observations.

Since the tidal motion in the Japan Sea is relatively weak (Odamaki, 1989; Morimoto *et al*., 2000a), the near-inertial oscillations dominate in the deep water. Takematsu *et al*. (1999a) showed that the clockwise components had a sharp peak at an inertial period of about 18 hours at mooring site M5 (the location is shown in Fig. 1), but no peaks appeared at tidal periods such as diurnal or semidiurnal periods. Thus, it is relatively less complicated to detect the near-inertial oscillations here than in other oceans/seas.

Internal waves are responsible for diapycnal mixing, which is most effective when these waves are breaking. The energy of the near-inertial oscillations responsible for producing the homogeneity of the JSPW must also be non-negligible. Some studies have been carried out on the near-inertial oscillations in the Japan Sea (e.g., Lie, 1988; Kim *et al*., 2001; Park *et al*., 2004). From these, it is well known that there are significant near-inertial motions in the Japan Sea. However, the detailed characteristics, such as the temporal/spatial variabilities over the Japan Sea, are still poorly understood. In this study, we bring the near-inertial oscillations in deep water into focus, and describe their general characteristics.

2. Data

Moored current measurements have been carried out in the CREAMS (Circulation Research of East Asian Marginal Seas) program since 1993 to investigate the structure of the deep circulation of the Japan Sea. Figure 1 shows the mooring sites. Most of the sites lie in the southern Japan Sea, especially in the Yamato Basin. There are different numbers of current meters (Aanderaa RCM 7/8) on each mooring line at each site, with a maximum of three, all of them being in the JSPW. Since we are interested in deeper currents, the data from the deepest measurements for each mooring were used in this study. A description of these moorings is given in Table 1. Most of the mooring durations are one year, but some are moored for two or three years. For the data collected for over one year, the current meters were recovered and redeployed at the same position every year. A linear interpolation was used to account for missing data over time periods of a few days resulting from recovery and re-deployment. There were some datasets of less than one year due to missing data. Although temperature was also measured, it was not analyzed in this study, since the amplitude was too small to be able to discern any variation. We used an additional measurement taken by Hokkaido University (the mooring site HU), which is the same as that used in Mori *et al*. (2001). The data sampling interval was one hour, except for at HU. Since the data at HU were recorded every 30 minutes, these were averaged every hour and subsampled once per hour for consistency.

Data collected over longer durations would be useful for investigating the temporal (seasonal) variations. The longest mooring duration was three years, at sites

Table 1. Locations, depths, and periods of each mooring site.

Mooring	Latitude (N)	Longitude (E)	Instrument depth (m)	Date	Duration (year)
M1	43°43.0′	137°54.7′	2500	17 Aug. 1993–12 Jul. 1994	1
M2	40°41.5′	136°14.5′	2500	19 Aug. 1993–14 Jul. 1994	1
M3	41°19.7′	134°21.7′	3000	21 Aug. 1993–3 Aug. 1996	3
HU	40°36.6′	139°21.5′	2100	2 Apr. 1994–3 Apr. 1995	1
M4	41°18.0′	132°24.0′	2900	17 Jul. 1994–4 Aug. 1995	1
M5	39°38.0′	132°25.0′	2400	18 Jul. 1994–9 Aug. 1996	2
A3	36°22.9′	134°55.4′	680	27 May 1995–28 Mar. 1997	1.8
M6	42°24.9′	133°33.8′	2350	1 Aug. 1995–4 Aug. 1996	1
M7	41°45.0′	132°13.0′	1990	4 Aug. 1995–7 Aug. 1996	1
Y1	37°38.4′	134°47.1′	2770	16 Jun. 1997–8 Jun. 1998	1
Y2	37°39.5′	135°21.4′	2800	16 Jun. 1997–8 Jun. 1998	1
Y3	38°02.2′	135°03.3′	2850	16 Jun. 1997–8 Jun. 1998	1
D6	36°20.7′	132°08.0′	1450	15 Jun. 1998–7 Jun. 2001	3
C9	38°40.0′	133°40.7′	1210	13 Jun. 1998–9 Jun. 2000	2
B2	37°25.7′	135°39.8′	2580	13 Jun. 1999–11 Jun. 2000	1
B4	37°59.4′	135°02.5′	1990	13 Jun. 1999–10 Jun. 2000	1
C5	37°21.0′	133°38.6′	1400	17 Jun. 1999–8 Jun. 2000	1
X	37°30.0′	133°30.0′	1330	8 Jun. 2000–31 Jan. 2001	0.6
Y	38°20.0′	136°30.0′	2040	10 Jun. 2000–9 Jun. 2001	1
CM7	37°20.2′	133°40.8′	1500	8 Jun. 2001–15 Jun. 2002	1
CN3	37°40.9′	133°60.0′	1590	12 Jun. 2001–13 Jan. 2002	0.6
E5	37°32.4′	132°19.1′	1480	23 Jun. 2002–21 Jun. 2003	1
CG4	37°38.3′	133°21.6′	1480	22 Jun. 2002–21 Jun. 2003	1
CM6	37°20.7′	133°41.4′	1480	21 Jun. 2002–27 Jun. 2003	1

M3 and D6. M3 is located in the center of the Japan Basin. At this site, three current meters were deployed at depths of 1000, 2000, and 3000 m and all of the meters recorded the current velocities and directions throughout the three years. D6 was in the southeast of the Ulleung Basin. Two instruments were deployed at D6 at depths of 1000 and 1450 m, but only the instrument at a depth of 1450 m was maintained for three years. We can investigate the differences in the characteristics of near-inertial oscillations at these moorings by comparing them with each other, though the observation times were quite different. Moreover, we used all of the data shown in Table 1 to investigate the horizontal power distributions and the seasonal variations of the near-inertial oscillations.

The hydrographic data observed by R/V *Hakuho Maru* of the Ocean Research Institute, University of Tokyo, were also used to observe the vertical structure of the potential density. The observation was carried out during October 14–19, 2002, and is depicted by Line A in Fig. 1.

3. Analysis Method

3.1 Spectral analysis

The rotary FFT (Fast Fourier Transform) method used in this study requires $N = 2^p$ data samples (p is a positive integer) (Emery and Thomson, 2001). The three-year datasets at M3 and D6 were divided into three segments. Each segment has a one-year record and satisfies $N = 2^{13}$, which is almost the same as the number of the one-year samples. We calculated the rotary spectra for each year and then averaged them. The time series of the rotary spectra (referred to as dynamic spectra) were also calculated to investigate the temporal variation of the periodic motions. Here, a segment itself has data for $N = 2^{10}$ (~43 days) and has an overlap of 21 days. The clockwise components were calculated in each segment as the dynamic spectra.

3.2 Slab model

In order to investigate the influence of the wind stress

on the near-inertial oscillations and the temporal/spatial variabilities, a slab model (e.g., Pollard and Millard, 1970; D'Asaro, 1985) was used to estimate the injection of energy into the surface mixed layer. The model and the computation method are described in detail in D'Asaro (1985) and are introduced briefly here. The model equation is

$$\frac{dZ}{dt} + \omega Z = \frac{T}{H}, \tag{1}$$

written in terms of the complex quantities,

$$Z = u + iv, \tag{2}$$

$$T = \frac{\tau_x + i\tau_y}{\rho}, \tag{3}$$

and

$$\omega = r + if. \tag{4}$$

Here f is the inertial frequency, τ_x and τ_y are the wind stress components, H is the surface mixed layer thickness, ρ is the density, and r is the damping parameter. Since steady winds produce Ekman transport such that

$$Z_E = \frac{T}{\omega H}, \tag{5}$$

the inertial oscillation components can be expressed as

$$Z_I = Z - Z_E \tag{6}$$

$$\frac{dZ_I}{dt} + \omega Z_I = -\frac{d(T/H)}{dt}\frac{1}{\omega}. \tag{7}$$

The energy equation is obtained by multiplying (7) by Z_I^*, the complex conjugate of Z_I,

$$\frac{d\left(\frac{1}{2}\rho H|Z_I|^2\right)}{dt} = -r\rho H|Z_I|^2 - \mathrm{Re}\left[\rho\frac{Z_I}{\omega^*}\frac{dT^*}{dt}\right], \tag{8}$$

where the second term on the right-hand side represents the inertial energy flux (F_{wind}). ECMWF (European Centre for Medium-range Weather Forecasts) wind data with a time interval of 6 hours from 1993 through to 2000 were used to drive the model, assuming constant H = 50 m and $1/r$ = 4 days. It should be noted that the low temporal resolution (Δt = 6 hours) results in underestimations of at least 20% in terms of the energy flux. Nevertheless, the model results are adequate for qualitative analysis (D'Asaro, 1985; Shcherbina *et al.*, 2003).

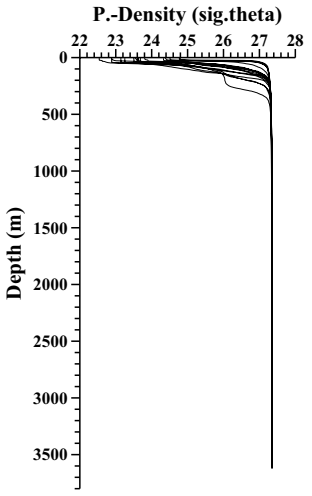

Fig. 2. Vertical profiles of potential density at all of the stations along Line A.

4. Results

4.1 Density profile

Vertical profiles of potential density at all 18 stations along Line A are shown in Fig. 2. As mentioned above, it can be seen that the JSPW is highly homogeneous, i.e., the density ranges from about 27.34–27.35σ_θ for depths below 500 m. Moreover, regional differences are not seen except in the upper layer. Although the observation points do not cover all of the Japan Sea, Line A extends from the south to the north of the Japan Sea, comprising the Ulleung, Yamato, and Japan Basins. It can therefore be concluded that the density of the JSPW is almost uniform both horizontally and vertically in the deep water of the Japan Sea.

4.2 Differences between M3 and D6

4.2.1 Currents

Unfiltered current vector plots at M3 and D6 are shown in Fig. 3. The remarkable feature at M3 is that the deep currents had eddy-like variations with eventfulness. Takematsu *et al.* (1999b) investigated the current fluctuations at M3 using SST imagery and drifter tracks, showing that the currents at 1000, 2000, and 3000 m were highly coherent throughout the observation period and the isolated anticyclonic eddies occasionally passed through M3. These eddies would have been barotropic/quasi-barotropic in nature and responsible for some of the variations.

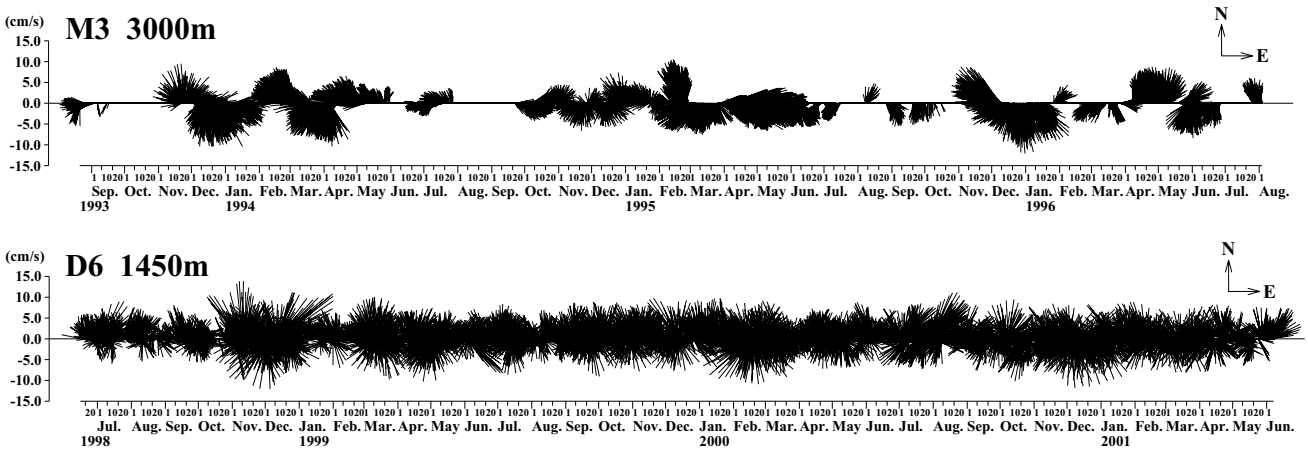

Fig. 3. Stick vector plots at M3 and D6. Data are unfiltered.

In contrast, the current at D6 is characterized by continuous fluctuations. The flow was constantly rotating with a speed of around 5–10 cm/s. The current variation at the 1000-m depth from June 1999 to June 2000 (not shown) was similar to that at the 1450-m depth. This implies that the deep currents at D6 were also vertically coherent.

4.2.2 Rotary spectra

Rotary spectra of currents at M3 and D6 are shown in Fig. 4. The near-inertial peak in the clockwise components is prominent in each of the measurements. The clockwise components also have small peaks at around $2f$ (where f is the local inertial frequency). These spectral characteristics are common at all the other sites, indicating that the near-inertial oscillations are the most dominant motion in the deep water of the Japan Sea. The level of power spectra is rather different from the Garret and Munk internal wave spectrum (Munk, 1981), which could be because the vertical profile of Brunt-Väisälä frequency in the Japan Sea is peculiar, as expected by the profile of the potential density shown in Fig. 2. There are four other peaks at tidal periods (O_1, K_1, M_2, S_2) at D6, especially in the anticlockwise components, but no tidal peaks are significant at M3, which is also shown by Senjyu *et al.* (2005) for D6 and Takematsu *et al.* (1999b) for M3. The continuous current variation at D6 seen in Fig. 3 is likely to be due to the tides. Since D6 is located near the Tsushima Strait, the variations in currents at D6 seem to be influenced by the tidal currents outside the Japan Sea.

4.2.3 Dynamic spectra

Figure 5 shows the dynamic spectra of clockwise current components at M3 and D6. There is an apparent annual variability at M3, that is, near-inertial oscillations at M3 become energetic during December. The power spectra at $2f$ were large during winter, too. The characteristics of the dynamic spectra at D6 show a different

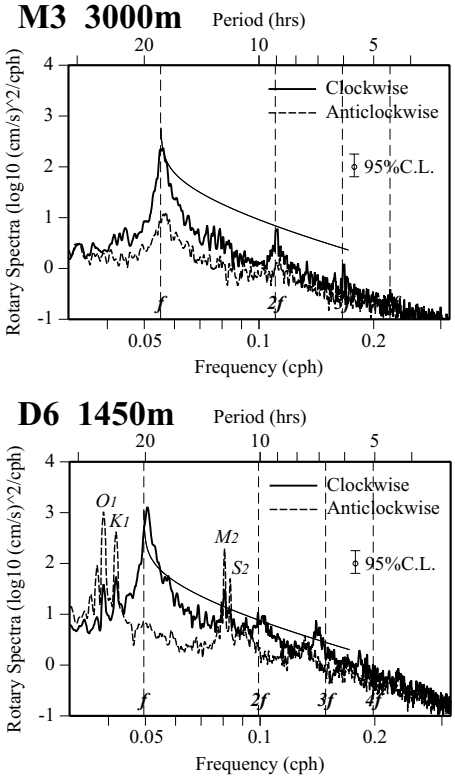

Fig. 4. Rotary spectra of the current velocities at M3 and D6. For comparison with the open ocean, the canonical Garret and Munk internal wave spectrum is depicted by the thin solid line.

aspect from those at M3. The variations in the power spectra show no distinct annual variation.

To verify the existence of the temporal variability, the deviations in the dynamic spectra are shown in Fig.

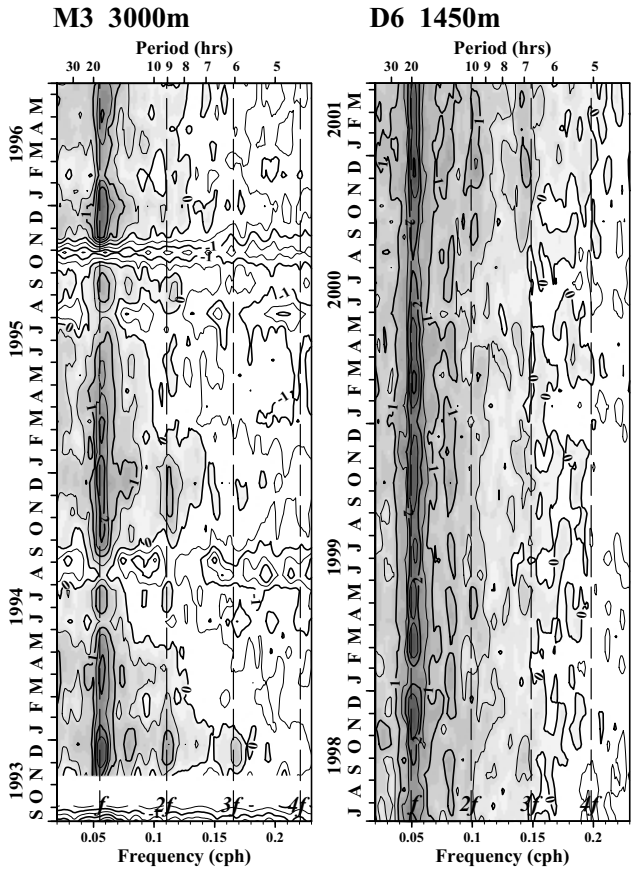

Fig. 5. Dynamic spectra of the clockwise component at M3 and D6. Values are expressed in terms of the common logarithm. Contour interval is 0.5.

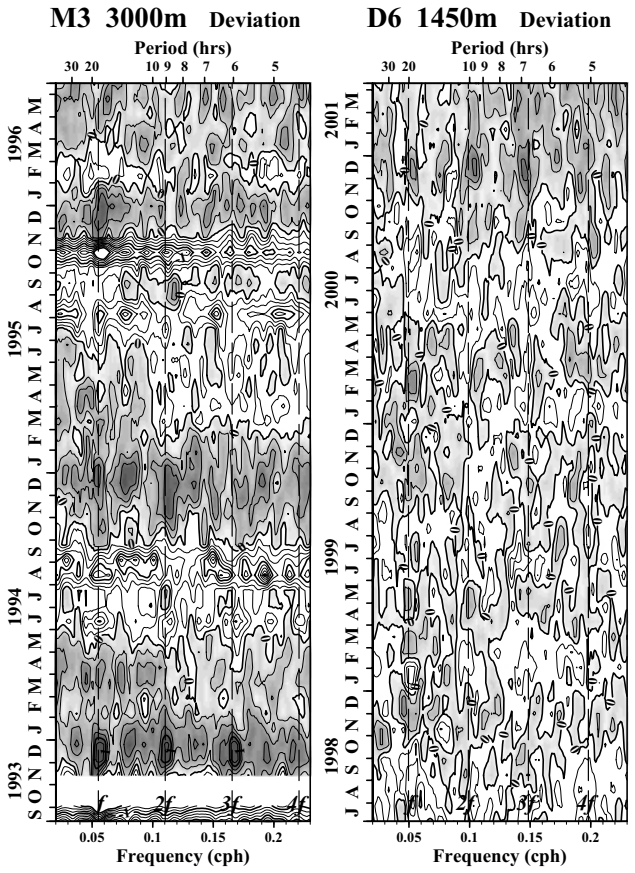

Fig. 6. Deviations in the dynamic spectra at M3 and D6, the anomalies from three-year averages at each frequency. Contour interval is 0.25.

6. These are the power anomalies from the three-year average at each frequency. At M3, there is a clear annual cycle, not only at the near-inertial frequency but also at other, higher frequencies. This implies that a range of high-frequency fluctuations became energetic in deep water in winter in addition to the near-inertial oscillation. However, the anomalous variations at D6 show no distinct seasonality throughout the three years. A close inspection of Fig. 6 indicates that there are enhanced fluctuations during the winter at D6, but the amplitude is not as large as that seen at M3. Since winter is a very windy season in the Japan Sea region, the annual variation with wintertime intensification is likely to be related to the seasonal wind over the Japan Sea. The relationship between the variations of the near-inertial oscillation and the wind will be discussed later.

4.3 Spatial distribution

Although the mooring sites at M3 and D6 may not be representative of the northern and the southern Japan Sea, it is suggested that the characteristic of the near-inertial oscillations varies spatially. Further investigations into the spatial distribution of the near-inertial oscillations were required. The rotary spectra in the clockwise components were calculated for every month and averaged for each season, that is, for spring (March–May), summer (June–August), fall (September–November) and winter (December–February). The peak values at the near-inertial frequency were picked out from the calculated rotary spectra. Figure 7 shows the horizontal distributions of the near-inertial peaks for each season. The circle diameter is proportional to the peak power. The peak values in the common logarithm and the ratios of the near-inertial peak frequency (ω_p) to local inertial frequency (f) are listed in Table 2. The near-inertial oscillations are generally more energetic in the southern Japan Sea and during the winter. A distinctive feature is seen in the Yamato Basin: the near-inertial peaks are extremely low in spring. Figure 8 shows the time series of the monthly averaged peaks in the northern and southern Japan Sea (including the Yamato Basin), the Yamato Basin, and at M3 and D6 to examine the spatial differences. As seen in

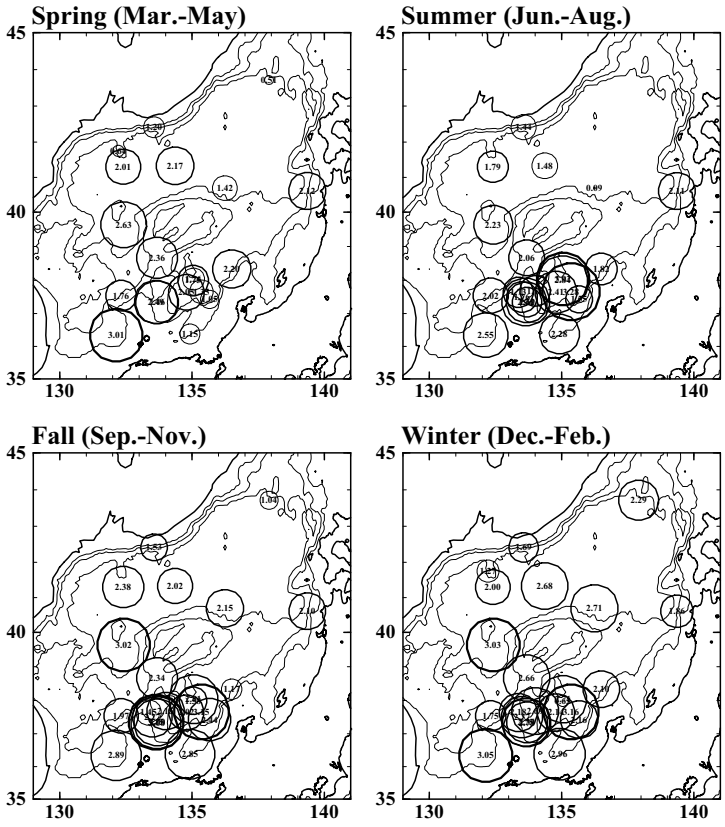

Fig. 7. Distribution of the near-inertial peaks calculated by rotary spectra during each season. Values are expressed in terms of the common logarithm. Circle diameter is proportional to the value.

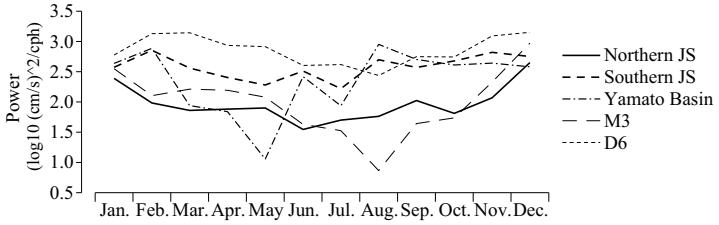

Fig. 8. Monthly averaged near-inertial peaks in the northern and southern Japan Sea, Yamato Basin, and at M3 and D6.

Fig. 7, the powers of the near-inertial oscillations often become intensified during the winter. The inertial oscillations in the northern Japan Sea appear to be less energetic than those in the southern part throughout the year, but the power in the northern part is comparable to that in the southern part during winter (January and December). The time series of the power at M3 and D6 also have an annual cycle, although the phases are different from the regional average. At D6, the magnitude is larger but the amplitude of the seasonal variation is smaller than that at M3. On the other hand, the temporal variation in the Yamato Basin is rather different from the others: the minimum appears in May. This variation seems to be overlapped by an annual cycle with wintertime intensification. Therefore, the structure of near-inertial oscillations observed in the Yamato Basin seems to have a specific mechanism.

5. Discussion

Moored current measurements have been conducted at 24 locations in the Japan Sea during the past ten years. However, the mooring periods were different and only a few of the moorings were deployed at the same time (see Table 1). Some characteristics of the temporal/spatial

Table 2. Near-inertial peak value in terms of the common logarithm shown in Fig. 9 and ratio of the near-inertial peak frequency (ω_p) to the local inertial frequency (f).

	Spring		Summer		Fall		Winter	
	Power	ω_p/f	Power	ω_p/f	Power	ω_p/f	Power	ω_p/f
Japan Basin								
M1	0.51	1.00	—	—	1.04	1.03	2.29	1.03
M2	1.42	1.09	0.09	1.00	2.15	1.03	2.71	1.02
M3	2.17	1.06	1.48	1.08	2.02	1.01	2.68	1.02
M4	2.01	1.01	1.79	1.07	2.38	1.03	2.00	1.03
M6	1.20	1.05	1.44	1.00	1.53	1.18	1.69	1.06
M7	0.64	0.96	—	—	—	—	1.27	1.04
HU	2.12	1.02	2.11	1.04	2.10	1.05	1.86	1.12
M5	2.63	1.02	2.23	1.01	3.02	1.01	3.03	1.02
Ulleung and Yamato Basins								
E5	1.76	1.09	2.02	1.06	1.97	1.08	1.75	1.10
D6	3.01	1.03	2.55	1.04	2.89	1.04	3.05	1.04
C9	2.36	1.07	2.06	1.07	2.34	1.07	2.66	1.04
CG4	—	—	1.73	1.08	1.45	1.01	2.18	1.02
X	—	—	1.76	1.05	2.27	1.09	2.37	1.06
C5	2.49	1.03	2.74	1.04	3.15	1.05	2.75	1.03
CM7	2.46	1.03	2.32	1.04	3.00	1.05	2.78	1.04
CM6	—	—	1.69	1.07	2.70	1.05	2.34	0.95
CN3	—	—	1.75	1.05	2.15	1.10	2.69	1.03
A3	1.15	0.95	2.28	1.07	2.85	1.06	2.96	1.08
Y1	2.05	1.03	2.41	1.08	2.02	1.06	2.14	1.03
Y2	1.35	0.94	3.28	1.02	3.15	1.05	3.16	1.05
Y3	1.26	1.06	3.02	1.08	2.81	1.02	2.71	1.04
B4	1.75	1.02	2.84	1.03	1.58	1.04	0.65	1.12
B2	1.05	0.96	1.55	1.09	2.44	1.05	2.16	1.07
Y	2.20	1.11	1.82	1.06	1.17	1.13	2.10	1.04

variability came to light as a result of this sparse data set. According to the analysis of the current velocities at M3 and D6, the seasonal wind seemed to reflect the variations in the near-inertial oscillations at only M3. The mooring data also show that the near-inertial oscillations were more energetic in the southern part of the subpolar front. A few plausible explanations for the temporal/spatial variations in the near-inertial oscillation in the deep water of the Japan Sea are discussed below.

5.1 Wind stress

To estimate the energy flux from the wind to the inertial oscillations in the surface mixed layer, the simple slab model was used, as introduced in Subsection 3.2. Figure 9 illustrates the distributions in the wind-induced inertial energy input per unit surface area for each season, averaged over eight years from 1993 through to 2000. The energy is susceptible to seasonal variations in the wind, and the estimated energy in the winter is about ten times larger than that during the summer. In this case, we let H be constant. In practice, the surface mixed layer thickness in the Japan Sea is changing both spatially and temporally. Nevertheless, H was set as a constant over time and location in order to isolate the effect of the wind stress.

The distribution of the energy injection is not horizontally uniform, except for during the summer. The relatively energetic regions are seen west of the Yamato Rise, south of the Yamato Basin and in the easternmost part of the Japan Sea at around 40°N during the winter. The seasonal variation responds faithfully to the wind, and the least energetic season is summer.

Figure 10 shows the time series of the energy fluxes from the wind to the inertial currents in the surface layer calculated by the slab model (F_{wind}) and the time differentials of the near-inertial energy ($\Delta E_{IC}/\Delta t$) at M3 and D6. Here, E_{IC} is the kinetic energy of the near-inertial oscillation and Δt is the sampling interval (=1 hour). E_{IC} was estimated from processed data using a band-pass filter designed by Kaiser and Reed (1977). The filter response factor indicates that almost 100% of the input values could be filtered, and that the amplitude of the near-

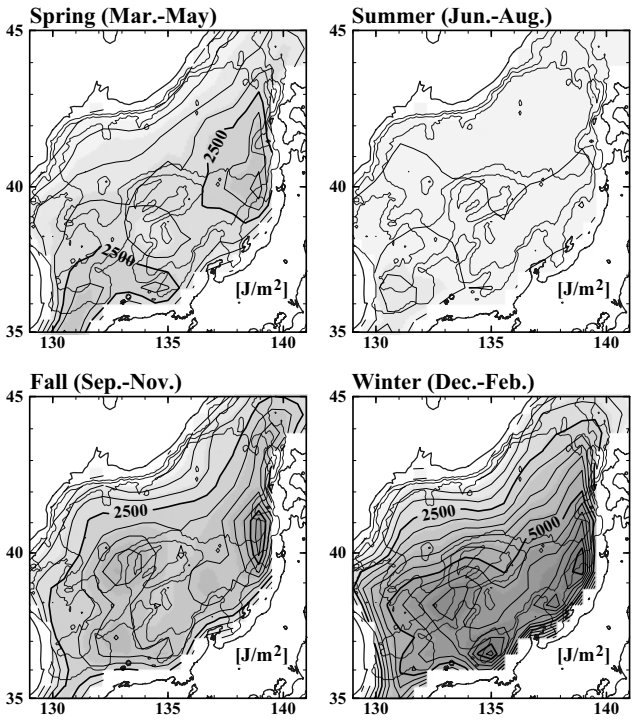

Fig. 9. Map of estimated energy of injection from the wind stress into the surface mixed layer, estimated by the slab model. Contour interval is 500 J/m^2.

inertial oscillations reaches a peak with a maximum of about 6 cm/s at both sites (not shown). The explicit relationship between F_{wind} and $\Delta E_{IC}/\Delta t$ is not seen at either site, but the energy injections become rather high during winter at both sites, which correspond to the wintertime intensification of the near-inertial oscillation, especially at M3. In order to highlight the long-time variation in the energy, the monthly integrals of F_{wind} and the positive value of $\Delta E_{IC}/\Delta t$ are plotted in Fig. 11. For the overall period, except for the last winter of measurements at M3, the variation and amplitude of the energy flux of near-inertial oscillations in deep water are in agreement with that of the surface energy flux induced by the wind. Thus, the inertial waves in the surface mixed layer due to the wind forcing might partly account for the source of the near-inertial oscillations in deep water, at least for long time scales such as seasonal variations, especially at M3.

It might therefore be possible to estimate how the energy of the inertial motions indicated by the slab model propagates downward to the deep water. Figure 12 shows the spatially averaged monthly integrals of F_{wind}, which are averaged over eight years from 1993 through to 2000, and that of the positive value of $\Delta E_{IC}/\Delta t$ at each mooring, which indicate the injected energy in the deep water in the northern and southern Japan Sea (including the Yamato Basin) and the Yamato Basin. The modeled energy flux has an apparent annual cycle with wintertime enhancement, which corresponds to the seasonal variability of the energy flux of the near-inertial oscillations in the deep water. In the Yamato Basin, however, the energy flux in the deep water is large not only in winter but also in summer and fall. It is rather hard to evaluate the amount of energy from wind-induced inertial motions in the surface layer that is transferred to the deep water when the energy flux is low, that is, from spring to fall. The energy injection of the inertial oscillations induced by the wind into the deep water could be estimated to be about 500 J/m^2/month in winter in the Japan Sea, which corresponds to the order of 10^{-10} W/kg if the height of the water column is assumed to be 2000 m. This estimated value is about half and 30% of the wind-induced energy flux in winter in the northern Japan Sea and the Yamato Basin, respectively. Since the near-inertial oscillations in the deep water would be induced by multiple sources, this estimation can be recognized only as a rough value. The vertical/horizontal energy propagation process needs to be investigated in future studies to reveal in detail the relationship between the wind and the near-inertial oscillations in deep water.

5.2 Surface current

Because there are ordinarily some eddies/meanders moving eastward in the southern Japan Sea (e.g., Isoda, 1994), the flow pattern of the surface current is expected to be greatly variable. Fluctuations in the baroclinic currents could induce the internal waves and the near-inertial oscillations, and its energy could be trapped and then propagate downward to the deep water in regions of negative relative vorticity (e.g., Blumen, 1972; Moores, 1973; Kunze, 1985). Figure 13 shows the standard deviations of the sea surface height (SSH) anomalies during each season. This distribution was derived from the composition of the satellite altimetric data of the TOPEX/Poseidon and the ERS during October 1992–October 2001. The tidal components have already been removed from these data. The rather steep gradient lies zonally at 39–40°N, corresponding to the subpolar front. The standard deviation north of the subpolar front is around 4 cm, but that in the southern area is about 6–10 cm with a maximum of 12 cm in the Yamato Basin (38°N, 135.5°E) during the fall. Moreover, the SSH is less variable in spring. Morimoto *et al.* (2000b) reported the time series of the number of eddies in the north and south of the subpolar front from May 1995 to July 1997. There were more eddies in the southern Japan Sea than in the northern part, and the minima appeared during spring. Lee *et al.* (2000) demonstrated that the eddy kinetic energy of the surface layer also marked larger values in the Yamato Basin. These evidences show, in other words, that the fluctuations of

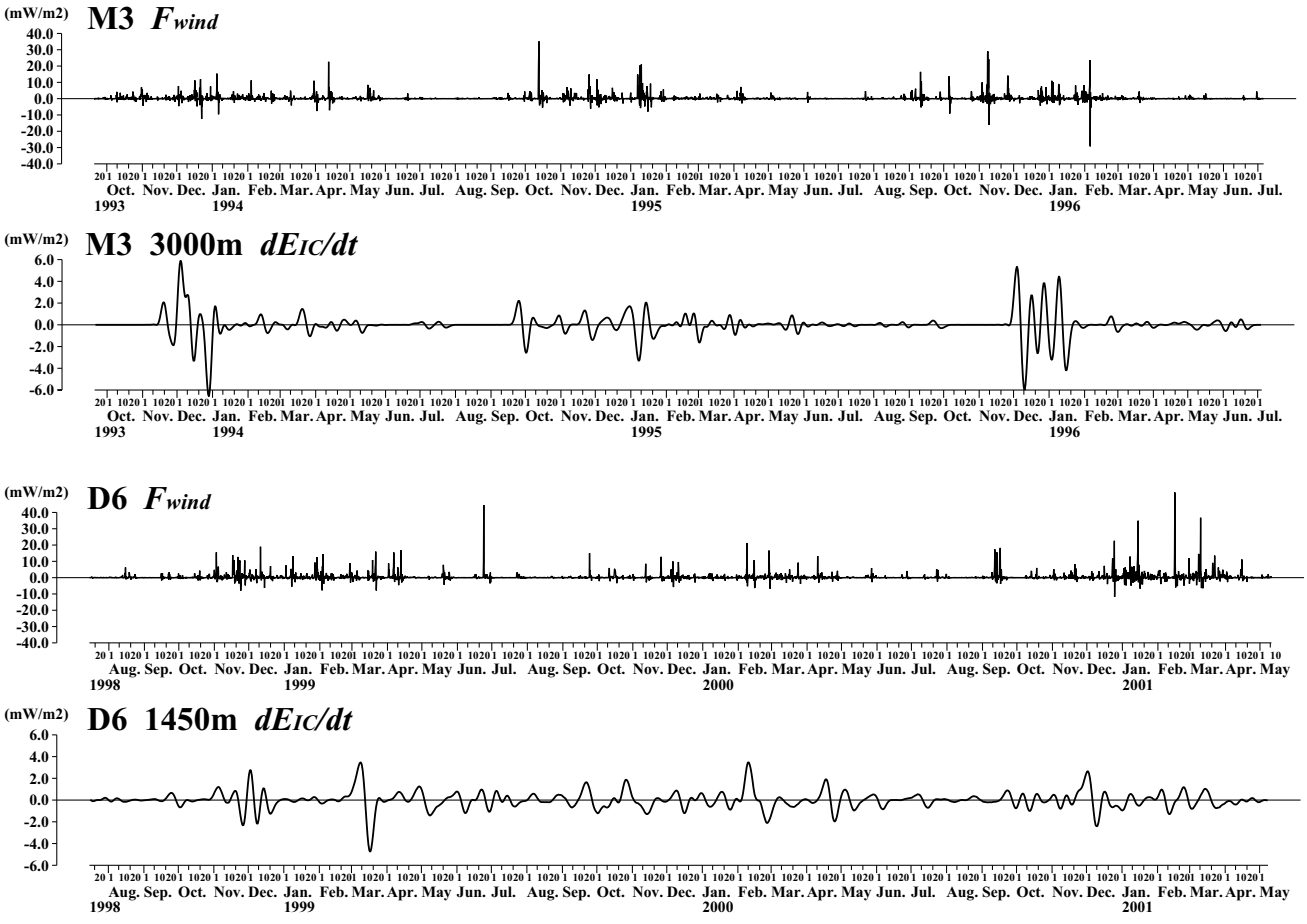

Fig. 10. Energy flux from the wind to the inertial currents in the surface layer estimated by the slab model (F_{wind}) and time differential of the near-inertial energies ($\Delta E_{IC}/\Delta t$) at site M3 and D6.

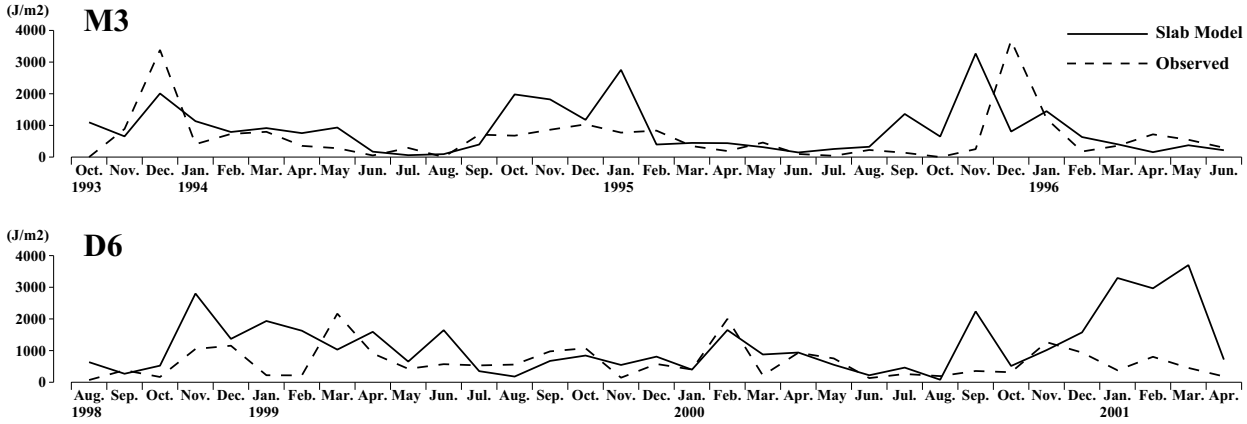

Fig. 11. Monthly integrals of F_{wind} and positive value of $\Delta E_{IC}/\Delta t$ at M3 and D6.

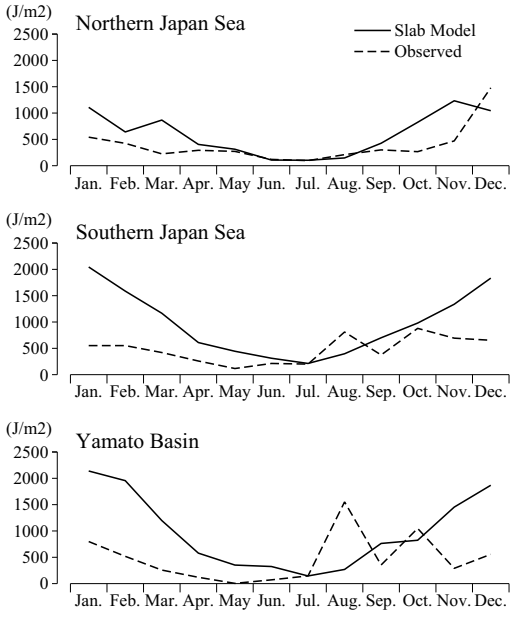

Fig. 12. Monthly integrals of F_{wind}, averaged over eight years from 1993 through to 2000, and averaged monthly integrals of positive value of $\Delta E_{IC}/\Delta t$ at each mooring in the northern and southern Japan Sea and the Yamato Basin.

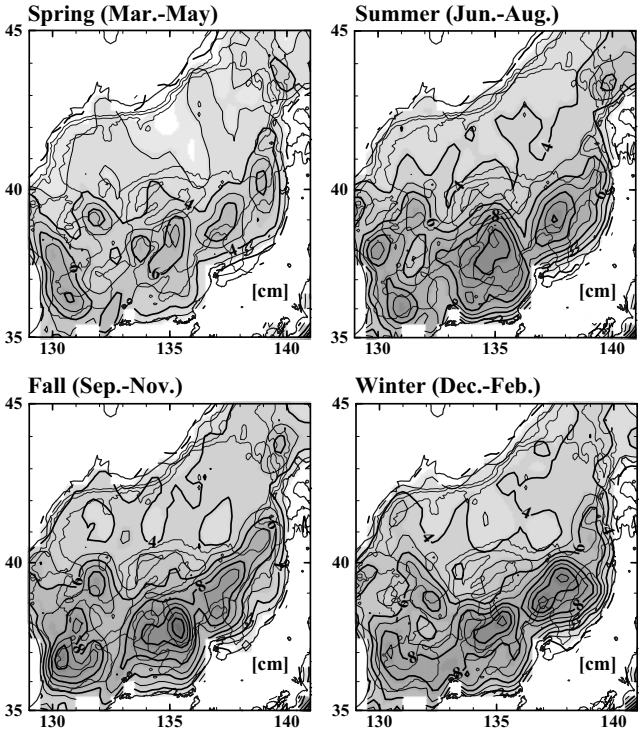

Fig. 13. Standard deviation of the SSH anomaly in each season. Contour interval is 1 cm. Tidal components were removed in the altimetric data.

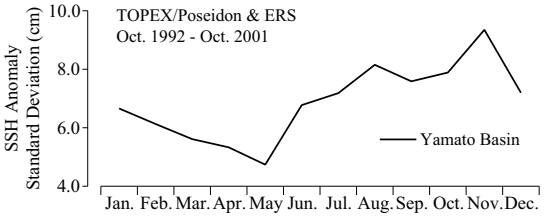

Fig. 14. Ten-year averaged annual variation of standard deviations of the SSH anomaly in the Yamato Basin area (36.5°N, 133.5°E–39.0°N, 137.0°E).

the surface currents are more active in the southern Japan Sea, especially in the Yamato Basin, and less during spring than in other seasons.

The ten-year averaged annual variation of the standard deviations of the SSH anomaly in the Yamato Basin region (36.5°N, 133.5°E–39.0°N, 137.0°E) is shown in Fig. 14. The standard deviation is at its lowest during May, corresponding to when the near-inertial oscillations in the deep water of the Yamato Basin were less energetic (see Fig. 8). In order to see the relationship among the near-inertial oscillations, the wind, and the SSH in the Yamato Basin, their behaviors at Y1, Y2, and Y3 are investigated as an example for 1997–1998. Figure 15 shows the time series of F_{wind}, $\Delta E_{IC}/\Delta t$, and the SSH anomalies at Y1, Y2, and Y3. A significant fluctuation in $\Delta E_{IC}/\Delta t$ is seen around September 1997 at each site, whereas the energy injection from the wind indicated by the slab model is not as high during the summer as in the winter. On the other hand, the SSH anomalies are increasing in August and September, when the warm eddy was passing around these sites (Nagano, 2000). The amplitude of $\Delta E_{IC}/\Delta t$ at Y2 is about twice those at Y1 and Y3, but the reason could not be determined in this work.

The most energetic region for the near-inertial oscillations is generally in the Yamato Basin except during the spring (Fig. 7), whereas the result of the slab model (Fig. 9) shows that the Yamato Basin region takes slightly less energy from the wind stress than the ambient area. Since there are few current measurements in the upper layer above the main pycnocline, it is presently an open question how the near-inertial oscillation in the deep water of the Yamato Basin is excited. One possible explanation is that the current variation in the surface layer could be responsible for the intensification of the near-inertial motions in the deep water, especially in the Yamato Basin.

If we assume that the increase in kinetic energy flux during summer and fall in the Yamato Basin, as shown in Fig. 12, is due to the surface current variation, the active

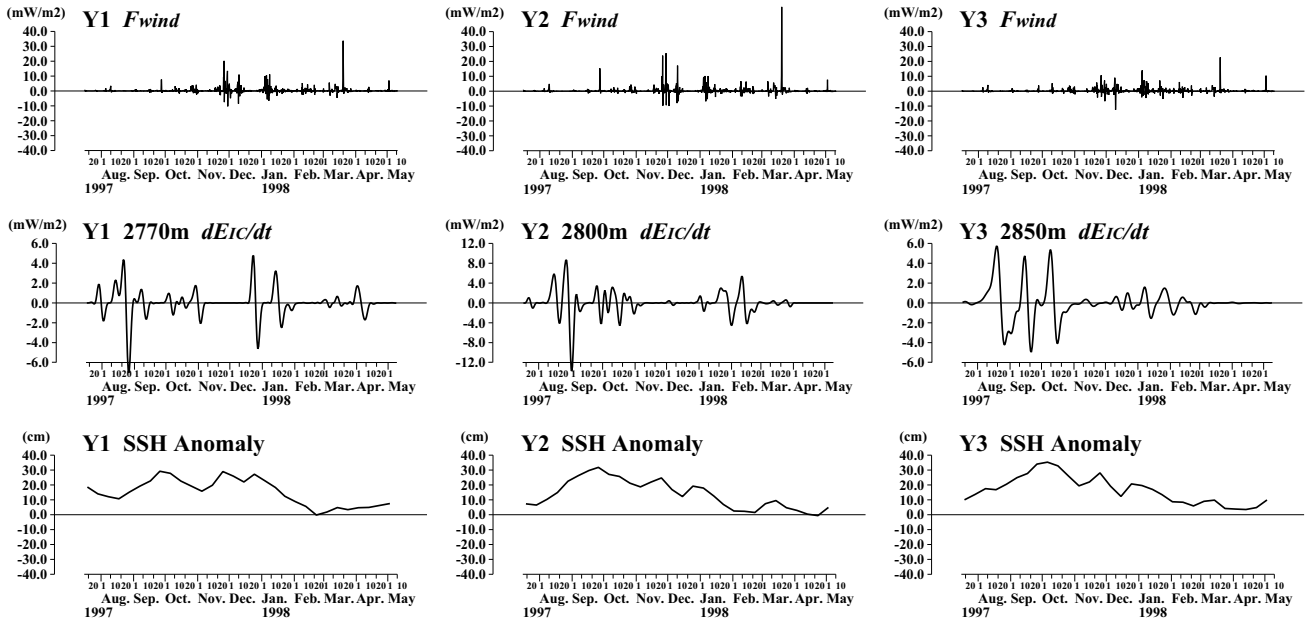

Fig. 15. Time series of energy flux from the wind to the inertial currents in the surface layer estimated by the slab model (F_{wind}), time differential of the near-inertial energies ($\Delta E_{IC}/\Delta t$), and SSH anomalies at Y1, Y2, and Y3.

fluctuations in the baroclinic currents could produce the energy with a maximum of about 1000 J/m^2/month for exciting the near-inertial oscillations in the deep water, as expected by the gap seen in Fig. 12 for the summer in the Yamato Basin. This value is twice as much as those of the estimated energy injection of the inertial oscillations induced by the wind into the deep water (see Subsection 5.1). Such a value, however, might be overestimated, since the wind-induced energy (F_{wind}) in summer would be underestimated due to the surface mixed layer thickness (H) in the slab model being large in summer (H is taken to be 50 m in this study) and the low temporal resolution, as mentioned in Subsection 3.2.

5.3 Topographic roughness and barotropic current

The bottom topography is complicated except for the Japan Basin (see Fig. 1). Such a rough bottom topography may be acting as an energy source for the near-inertial waves (e.g., Leaman, 1976). As seen in Figs. 5 and 6, the near-inertial oscillation at D6 is continuous but has some variation. The tides affect the current variations around the location of D6 (see Fig. 4). Also, as mentioned above, the deep flow is very energetic in the Japan Sea. The topography of the Japan Sea is therefore likely to produce some turbulence by the barotropic currents and must not be disregarded as a contributor to inducing the inertial oscillations in the deep water.

Furthermore, it must be considered that the barotropic current itself can cause the enhancement of the near-inertial oscillation in the deep water, since the variation in the near-inertial oscillations at M3 are likely to be accompanied by the passing of barotropic/quasi-barotropic eddies.

6. Conclusions

It has been shown that the near-inertial oscillations in the deep water of the Japan Sea vary both spatially and temporally.

1) The near-inertial oscillations are more energetic in the southern Japan Sea, i.e., the southern area of the subpolar front and also the Tsushima Current region.

2) The variation in the near-inertial oscillations has an annual cycle with wintertime intensification corresponding to the seasonal wind.

3) In the Yamato Basin, the aspect of such variations is different from other areas: the near-inertial oscillations are less energetic during the spring and more energetic during the summer.

The wind stress would not be the only definite source of energy for the near-inertial oscillation in the deep water of the Japan Sea. Other sources have been proposed here, but are supported only by circumstantial evidence. This study is the first phase in investigating the properties and structures of the near-inertial oscillations in the deep water of the Japan Sea. Further analyses are needed into the mechanisms, such as the vertical coherency and the phase difference, which would explain the direction of the energy propagation. Further studies will focus on identifying the sources and the propagation processes.

Acknowledgements

The authors would like to thank the officers and crews aboard the T/S *Kakuyo Maru*, R/V *Prof. Khromov*, T/S *Oshoro Maru*, T/S *Hokusei Maru*, and R/V *Hakuho Maru* for their assistance in the operations. We are also grateful to the editor and anonymous reviewers for their valuable comments and helpful advice, to Dr. S. Varlamov and Dr. N. Hirose of RIAM, Kyushu University for their assistance in processing the wind data, to Dr. K. Ichikawa of RIAM, Kyushu University for providing the satellite altimetric data (J-OFURO), and to Mr. Tim Brierley for proofreading the manuscript. The wind data we used were provided by the European Centre for Medium-range Weather Forecasts.

References

Blumen, W. (1972): Geostrophic adjustment. *Rev. Geophys. Space Phys*., **10**, 485–528.

D'Asaro, E. A. (1985): The energy flux from the wind to near-inertial motions in the surface mixed layer. *J. Phys. Oceanogr*., **15**, 1043–1059.

Emery, W. J. and R. E. Thomson (2001): *Data Analysis Methods in Physical Oceanography: Second and Revised Edition*. Elsevier Science B.V., Amsterdam, 638 pp.

Isoda, Y. (1994): Warm eddy movements in the eastern Japan Sea. *J. Oceanogr*., **50**, 1–15.

Kaiser, J. F. and W. A. Reed (1977): Data smoothing using low-pass digital filters. *Rev. Sci. Instrum*., **48**, 1447–1457.

Kim, H. R., S. Ahn and K. Kim (2001): Observations of highly nonlinear internal solitons generated by near-inertial internal waves off the east coast of Korea. *Geophys. Res. Lett*., **16**, 3191–3194.

Kunze, E. (1985): Near-inertial wave propagation in geostrophic shear. *J. Phys. Oceanogr*., **15**, 544–565.

Leaman, K. D. (1976): Observations on the vertical polarization and energy flux of near-inertial waves. *J. Phys. Oceanogr*., **6**, 894–908.

Lee, D. K., P. P. Niiler, S. R. Lee, K. Kim and H. J. Lie (2000): Energetics of the surface circulation of the Japan/East Sea. *J. Geophys. Res*., **105**, 19561–19573.

Lie, H. J. (1988): Near-inertial current oscillations off the mid-east coast of Korea. *Prog. Oceanogr*., **21**, 241–253.

Moores, C. N. K. (1973): Several effects of a baroclinic current on the cross-stream propagation of inertial-internal waves. *Geophys. Fluid Dyn*., **6**, 245–275.

Mori, K., Y. Isoda, T. Murakami and K. Ohtani (2001): Low-frequency variations of the deep flow southwest of the Tsugaru Straits. *Umi no Kenkyu*, **10**, 1–13 (in Japanese with English abstract).

Morimoto, A., T. Yanagi and A. Kaneo (2000a): Tidal correlation of altimetric data in the Japan Sea. *J. Oceanogr*., **56**, 31–41.

Morimoto, A., T. Yanagi and A. Kaneo (2000b): Eddy field in the Japan Sea derived from satellite altimetric data. *J. Oceanogr*., **56**, 449–462.

Moriyasu, S. (1972): The Tsushima current. p. 353–369. In *Kuroshio: Its Physical Aspects*, ed. by H. Stommel and K. Yoshida, Univ. of Tokyo Press, Tokyo.

Munk, W. H. (1981): Internal Waves and small-scale processes. p. 264–291. In *Evolution of Physical Oceanography*, ed. by B. S. Warren and C. Wunsch, MIT Press, Cambridge.

Nagano, Z. (2000): Deep flow structures in the Japan Sea. Doctoral dissertation, Kyushu Univ., 100 pp. (in Japanese).

Naganuma, K. (1977): The oceanographic fluctuations in the Japan Sea. *Mar. Sci*. (*Kaiyo Kagaku*), **9**, 137–141 (in Japanese with English abstract).

Odamaki, M. (1989): Co-oscillating and independent tides of the Japan Sea. *J. Oceanogr. Soc. Japan*, **45**, 217–232.

Ohwada, M. and K. Tanioka (1972): Cruise report on the simultaneous observation of the Japan Sea in October 1969. *Oceanogr. Mag*., **23**, 47–58.

Park, J. J., K. Kim and W. R. Crawford (2004): Inertial currents estimated from surface trajectories of ARGO floats. *Geophys. Res. Lett*., **31**, doi:10.1029/2004GL020191.

Pollard, R. T. and R. C. Millard, Jr. (1970): Comparison between observed and simulated wind-generated inertial oscillations. *Deep-Sea Res*., **17**, 813–821.

Senjyu, T., H. R. Shin, J. H. Yoon, Z. Nagano, H. S. An, S. K. Byun and C. K. Lee (2005): Deep flow field in the Japan/East Sea as deduced from direct current measurements. *Deep-Sea Res*. (in press).

Shcherbina, A. Y., L. D. Talley, E. Firing and P. Hacker (2003): Near-surface frontal zone trapping and deep upward propagation of internal wave energy in the Japan/East Sea. *J. Phys. Oceanogr*., **33**, 900–912.

Suda, K., K. Hidaka, Y. Matsudaira, E. Kurashige, H. Kawasaki and T. Kubo (1932): The results of the oceanographical observations on board R.M.S. "Syunpu Maru" in the southern part of the Japan Sea in the summer of 1930. *J. Oceanogr. Imp. Mar. Observ*., **4**, 1–174 (in Japanese).

Takematsu, M., Z. Nagano, A. G. Ostrovskii, K. Kim and Y. Volkov (1999a): Direct measurements of deep currents in the northern Japan Sea. *J. Oceanogr*., **55**, 207–216.

Takematsu, M., A. G. Ostrovskii and Z. Nagano (1999b): Observations of eddies in the Japan Basin interior. *J. Oceanogr*., **55**, 237–246.

Tanioka, K. (1962): A review of sea conditions in the Japan Sea (II) On the cold, warm and saline water regions. *Umi to Sora*, **38**, 115–128 (in Japanese).

Uda, M. (1934): The results of simultaneous oceanographical investigations in the Japan Sea and its adjacent waters in May and June, 1932. *J. Imp. Fish. Exp. Sta*., **5**, 57–190 (in Japanese with English abstract).